Environmental Science: Atmospheres

ROYAL SOCIETY OF CHEMISTRY

PAPER

View Article Online
View Journal

Cite this: DOI: 10.1039/d6ea00012f

Microscopic characteristics and source identification of ambient particles based on electron microscopy: a case study of a steel city

Qian Liu,[a] Menghan Tong,[bc] Yatao Yang,[bc] Peng Zhao [db] and Pusheng Zhao *[bc]

Advances in computer-controlled scanning electron microscopy (CCSEM) technology allow large volumes of single-particle microscopic characteristic data to be acquired. Combined with big data analysis, this enables refined source apportionment of ambient particulate matter (PM). To meet particulate pollution prevention and control needs while evaluating this method's performance in source identification, this study selected Benxi, a typical steel industrial city, for ambient PM collection and single-particle source apportionment. Passive samplers collected samples at two sites (CT: Caitun; XH: Xihu) in winter, summer, and autumn 2023. Concentration monitoring showed that PM was higher in winter and lower in summer, and $PM_{2.5}$ at CT was generally higher than at XH. The particle size distribution presents obvious seasonal differences and the diurnal variation of particle concentration shows a bimodal pattern closely related to human activities and the evolution of the atmospheric boundary layer. By obtaining single-particle elemental compositions and microscopic image data through CCSEM technology, combined with methods such as clustering analysis, 10 major pollution source types were ultimately identified. Among these, soil dust (31.5%) and construction dust (17.4%) were the primary local pollution sources, while organic particles (20.4%) and coal-fired ash (8.2%) highlighted the significant roles of industrial emissions, combustion processes, and secondary formation. Size distribution characteristics indicated that particles associated with combustion, industrial emissions, and secondary formation (*e.g.*, biomass particles, carbonaceous particles, and metal particles) were mainly enriched in the fine particle fraction ($PM_{2.5}$), whereas fugitive dust sources (soil dust, construction dust, and salt particles) were dominated by coarse particles ($PM_{2.5-10}$). Significant differences in source contributions exist between the CT site affected by industry and residential activities and the XH site affected by mining activities. Influenced by steel mills, coking industries, and residential activities, the CT site showed prominent contributions from industrial and combustion sources to $PM_{2.5}$. In contrast, driven by mining and transportation activities, the XH site had higher contributions from fugitive dust. This study verified the effectiveness of CCSEM technology and big data analysis in the source identification of ambient PM in urban area, providing a scientific basis for formulating targeted pollution control strategies in Benxi and similar cities.

Received 23rd January 2026
Accepted 21st May 2026

DOI: 10.1039/d6ea00012f

rsc.li/esatmospheres

Environmental significance

Ambient particulate matter remains a critical environmental and public health challenge in China, where complex emission sources hinder effective pollution control. Accurately identifying particulate sources is essential for designing targeted mitigation strategies and achieving further reductions in $PM_{2.5}$ concentrations beyond current regulatory gains. This study applies computer-controlled scanning electron microscopy combined with big-data analysis to resolve particle-scale sources in Benxi, a typical steel-industry city. By identifying ten distinct particle source types and their size-resolved contributions, we demonstrate that fugitive dust dominates overall PM mass, while industrial, combustion, and secondary particles drive fine-particle pollution. These findings highlight the value of high-resolution single-particle approaches for supporting evidence-based air quality management in industrial regions.

Introduction

As pointed out in the white paper "China's Green Development in the New Era" released by the State Council Information Office, China has achieved remarkable progress in $PM_{2.5}$ control, with the average concentration dropping from 46 μg

[a]National Academy of Financial and Economic Strategy, Central University of Finance and Economics, Beijing, China
[b]Joint Laboratory for Electron Microscopy Analysis of Atmospheric Particles, Ministry of Ecology and Environment, Beijing, China. E-mail: zhaopusheng@bmet.cn
[c]Beijing Met High-Tech Co., Ltd, Beijing, China
[d]College of Environmental Science and Engineering, Nankai University, China

m^{-3} in 2015 to 30 μg m^{-3} in 2023, demonstrating the effectiveness of policy-led interventions. By 2024, approximately 75% of cities had met the national standard for $PM_{2.5}$ concentration (35 μg m^{-3} for annual average). However, to achieve the goal by 2035 (25 μg m^{-3}), over 60% of cities still need to greatly improve their particulate matter pollution. Moreover, there is a more significant disparity when compared to the World Health Organization (WHO) guidelines and international benchmarks. Going forward, particulate matter pollution prevention and control will remain a pivotal component of China's atmospheric pollution management strategy. The identification and quantitative analysis of particulate matter sources will continue to be central to achieving further reductions in $PM_{2.5}$ levels.

Receptor models,[1,2] including factor analysis or principal component analysis (such as Positive Matrix Factorization, PMF) and chemical mass balance (CMB), have emerged as the most widely applied techniques for source apportionment of atmospheric particulate matter. These methods derive particulate matter sources based on particle composition profiles encompassing carbon fractions, water-soluble ions, and inorganic elements through "bulk" analytical techniques.[3,4] However, constrained by the types of components and data volume, such methods are only capable of classifying pollution sources into a limited number of broad categories (such as industrial sources, fugitive dust, transportation sources, domestic sources, *etc.*). Furthermore, when using the factor analysis method, it is necessary to utilize the profiles of multiple samples (usually more than 50) to obtain one apportionment result, and these samples must also have significant differences in their sources.

Single-particle analysis[5,6] has emerged as a crucial international approach for characterizing the physical and chemical properties of atmospheric particulate matter. Scanning electron microscopy coupled with energy dispersive X-ray spectroscopy (SEM-EDS) is a powerful single-particle analytical tool capable of providing extensive detailed information on particulate matter, including its morphology, chemical composition, particle size, and mixing state. These characteristics can serve as a "fingerprint" for identifying the sources of individual particles.[7–9] Nevertheless, conventional electron microscopy single-particle analysis relying on manual operation is highly time-consuming and labor-intensive. Moreover, the limited number of particles that can be analyzed manually fails to adequately represent the actual pollution levels in the environment. As a result, for an extended period, research and applications of source apportionment based on single-particle electron microscopy data have remained relatively scarce.

Computer-controlled scanning electron microscopy (CCSEM)[10–14] enables the control of scanning electron microscopy and energy dispersive spectroscopy (SEM-EDS) as well as the automatic identification of particulate matter. It can quickly acquire detailed morphological and chemical composition data for individual particles (thousands of particles per hour). Based on such data, the category of each individual particle can be determined using classification rules or clustering analysis, allowing the contribution from different sources to any given environmental sample to be estimated.[15–19] In addition, the single-particle chemical compositions or classification results of different particle classes can also be used as a profile, and source apportionment tools (such as CMB and PMF) can be employed to further clarify their sources.[20] Deep learning methods have also been introduced, which help to leverage the advantages of big data obtained by CCSEM and enhance the precision of the source identification.[21,22]

All in all, compared with conventional bulk-analysis-based source apportionment methods, the CCSEM single-particle tracing approach offers substantial improvements in four key aspects: (1) data volume-while bulk analysis typically yields only 30–40 chemical components per set of samples, CCSEM examines thousands of particles per sample, with each particle providing dozens to hundreds of valid data points (images, size parameters, and composition), increasing the data volume by 4–5 orders of magnitude; (2) resolution-factor analysis methods (*e.g.*, PMF) require dozens of samples from the same site to produce a single apportionment result with only a few source categories, whereas single-particle tracing enables detailed size-resolved source apportionment from a single environmental sample; (3) efficiency-bulk analysis demands multiple instruments and is time-consuming and costly, whereas CCSEM requires minimal sample mass, operates rapidly, and is cost-effective; and (4) dimensionality-while mainstream apportionment techniques rely solely on chemical composition, single-particle analysis integrates morphological and size information, providing multi-dimensional particle characteristics.

Benxi, as a typical resource-based heavy industry city, has long relied on industries such as steel, coal, and chemicals for its economic development. In a bid to enhance regional air quality, the city has put in place a series of pollution abatement measures, such as ultra-low emission retrofits in the iron and steel sector, ecological restoration of mines, and comprehensive control of vehicle exhaust emissions. Monitoring data reveal that between 2019 and 2024, the $PM_{2.5}$ concentration in Benxi declined from 46 μg m^{-3} to 32.1 μg m^{-3}, a decrease of 30.2%. However, it still remains higher than the national average over the same period (29.3 μg m^{-3}), with particularly heavier pollution in winter, indicating that there is still potential for air quality improvement, which necessitates more refined identification and accurate quantification of particulate matter sources. In this study, intelligent electron microscopy analysis and big data identification technology were applied to investigate the physical and chemical properties and source apportionment of individual particles in Benxi in 2023. It aims to assess the specific performance of this technology in typical industrial cities and provide references and support for further pollution control efforts and similar initiatives in related cities.

Materials and methods

Sampling site and sample collection

For the purpose of conducting a refined source analysis of atmospheric particulate matter in Benxi, this study collected environmental single-particle samples during the periods of January–March 2023 (winter), August–September (summer), and October–November (autumn) (Table 1). The sampling sites

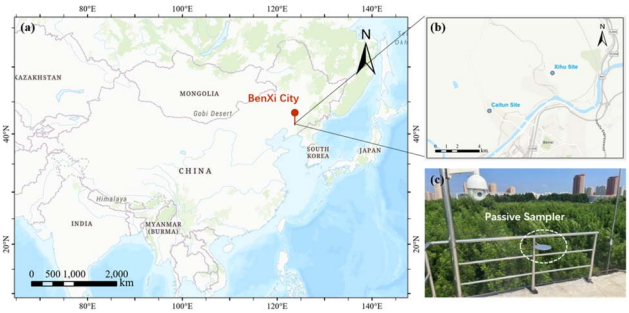

Fig. 1 Sketch of the sampling site: (a) location of Benxi city, (b) locations of two sampling sites, and (c) a passive sampler.

were arranged at two ambient air quality monitoring stations in Caitun (CT) and Xihu (XH) of Benxi (CT: 41.31°N, 123.72°E; XH: 41.33°N, 123.77°E) (Fig. 1). CT is an area with a large concentration of residents, and it is close to steel mills and coking plants. Around XH, there are coal mines, iron mines, and other mining areas, along with facilities associated with mining transportation.

Atmospheric particulate matter was collected using a passive sampler (UNC-PAS). This sampler operates without the need for operational maintenance, is unaffected by weather conditions, requires no external power supply, and allows for convenient filter replacement. Further details regarding the passive samplers are available in other sources.[23,24] Based on the principle of gravitational settling and diffusion, ambient air particulates deposited on the surface of polycarbonate (PC) membranes, which were then used for subsequent single-particle analysis.

Analytical procedure and data treatment

CCSEM analysis. In this study, an Intelligent Scanning Electron Microscope Environmental Particle Analysis System (IntelliSEM-EPAS) was employed for CCSEM analysis. This system automatically controls a Tescan Clara field-emission scanning electron microscope (FE-SEM) and two Bruker Xflash 6|60 energy-dispersive X-ray spectrometers (EDS). The analysis was performed in the backscattered electron (BSE) detection mode, with a working distance of 12 mm, an accelerating voltage of 20 kV and a beam current of 1 nA. Valid particles with a particle size range of 0.2–10 μm were screened out, and 90 rotated Feret measurements were conducted to obtain shape and size parameters. The electron beam was positioned at the centroid of each particle for a 1 second EDS spectrum acquisition. Ultimately, three shape parameters (projected area, perimeter, and grayscale intensity), five size parameters (average diameter, equivalent circle diameter, maximum diameter, minimum diameter, and diameter perpendicular to the maximum diameter), and 23 chemical elements (C, Na, Mg, Al, Si, Ca, Fe, S, K, Cl, Zn, Ba, V, Cr, Co, P, Se, Sn, Ti, Mn, Ni, Cu, and Pb) were obtained for each particle.

The analytical details have been described in our previous study.[19] A total of 61 086 valid particles were detected from 18 passive sampling samples, and the physical and chemical information of each particle-including microscope images, three shape parameters, five size parameters, and data on twenty-three elements-was automatically recorded in a database.

Data processing. Calculation of the concentration contribution: during passive sampling, the size distribution of the particles deposited on the membrane surface differs significantly from that in the actual environment. The reconstruction of concentrations and size contributions for particulate matter was based on the principle of passive sampling, with the application of a deposition velocity model.[23,24] Detailed descriptions of this model and calculation steps were provided in our previous work and are also compiled in the SI.[19]

Classification of particles: the classification of particle types primarily relied on the microscopic morphology and chemical compositions of ambient individual particles, following the steps below:

- Chemical composition clustering: the *k*-means was applied to cluster the chemical composition data of each particle obtained from the IntelliSEM-EPAS system.
- Determination of optimal cluster number: through cluster analysis with different cluster counts, 46 clusters were selected

Table 1 The duration of each sample period and the corresponding concentrations of $PM_{2.5}$, coarse particles, and PM_{10}; significant seasonal differences in PM concentrations were observed (ANOVA, $p < 0.001$), with winter > autumn > summer (Tukey HSD, all $p < 0.05$), while no significant difference was detected between the two sampling sites ($p > 0.05$)

	CT			XH		
Sample period	$PM_{2.5}$	Coarse particles	PM_{10}	$PM_{2.5}$	Coarse particles	PM_{10}
1.17–1.27	61.7	50.4	112.1	60.0	49.3	109.3
2.10–2.24	60.3	35.2	95.5	50.7	29.7	80.4
2.24–3.13	50.9	54.9	105.8	42.4	52.2	94.6
8.11–8.21	27.6	18.8	46.4	23.7	18.7	42.4
9.11–9.21	23.0	27.9	50.9	17.8	28.8	46.6
9.22–10.4	30.7	27.9	58.6	22.2	26.2	48.4
10.23–11.3	61.6	46.4	108	44.4	45.9	90.3
11.3–11.13	34.4	39.8	74.2	30.0	33.9	63.9
11.20–11.30	40.5	26.8	67.3	33.1	19.8	52.9

by minimizing the balance error and ensuring the representativeness of chemical components.

• Categorization into particle source types: based on the spectral similarity of EDS clusters, shape parameters, and also potential sources,[11,13,19,25,26] the 46 clusters were further grouped into 10 distinct particle source types: construction dust, soil dust, metal smelting particles, coal-fired ash, organic particles, carbonaceous particles, calcium–sulfur particles, sulfur-containing particles, salt particles, and biomass particles (Table 2).

This 10-category classification scheme represents a substantial refinement compared to conventional bulk-analysis-based source apportionment studies, which typically resolve only 4–6 broad source categories due to the limited chemical resolution of bulk data. The single-particle approach enables finer segregation of industrial sources that are often lumped together in traditional methods-for example, distinguishing coal-fired ash (high Si–Al–Fe–Ca, spherical) from carbonaceous particles (pure C, chain-like), or separating metal smelting particles (enriched in Fe–Mn–Zn–Pb) from construction dust (Ca-rich, irregular). Similarly, sulfur-containing particles (S-dominant, spherical) and calcium–sulfur particles (Ca–S co-enriched) are resolved as distinct types rather than being merged into a generic "secondary sulfate" category. This enhanced granularity is particularly critical for industrial cities like Benxi, where multiple emission–intensive activities (steel production, coal combustion, mining, and construction) coexist and require targeted control strategies. (Detailed clustering methods and classification criteria are provided in the SI).

A small number of particles that did not fit into the above 10 types were classified as "others". These "other" particles exhibited highly variable compositions and only accounted for 5% of the total particulate matter mass concentration, so they were excluded from subsequent discussions.

Quantitative apportionment of source contributions: to achieve quantitative source apportionment, the particle classification results were integrated with the concentration contribution values. On this basis, the absolute mass concentration ($\mu g\ m^{-3}$) and contribution ratio (%) of each particle type to the regional particulate matter pollution were calculated-directly reflecting the contribution of different pollution sources corresponding to each particle type at the sampling sites.

Statistical analysis. One-way ANOVA was used to assess seasonal differences in PM_{10} and $PM_{2.5}$ concentrations in winter, summer, and autumn. The Tukey HSD post-hoc test was performed when ANOVA was significant ($p < 0.05$). For site comparison, the paired-sample *t*-test was employed as the two sites were sampled simultaneously during the same periods (9 paired samples). All analyses were conducted using Python (scipy.stats and statsmodels libraries).

Results and discussion

PM concentrations

Based on the hourly automatic monitoring data from the CT and XH monitoring stations, the monthly average concentrations of both coarse particles ($PM_{2.5-10}$) and $PM_{2.5}$ were at relatively low levels in summer, while they increased in autumn and winter. In spring, affected by sand and dust weather, the concentration of coarse particles reached the highest level throughout the year. Among the two stations, the monthly average $PM_{2.5}$ concentration at CT was consistently higher than that at XH, whereas the difference in coarse particle concentrations between the two sites was negligible.

For this study, ambient particulate matter samples were collected during three periods: winter, summer, and autumn. Among these periods, the particulate matter concentrations were the highest in winter, with the average concentrations of

Table 2 Source type identification characteristics

Source type	Core elements	Microscopic morphological characteristics
Biomass particles	•Predominantly C and O, containing minor amounts of K, P, and other elements	•Irregular morphology with rough surfaces
Carbonaceous particles	•Predominantly C	•Amorphous structure; typical chain-like aggregates
Coal-fired ash	•High contents of Al and Si, containing metal and non-metal elements such as Fe, Ca, Mg, K, and Na, exhibiting multi-element mixed characteristics	•Three-dimensional spherical morphology
Construction dust	•Predominantly Ca	•Irregular morphology, blocky, flaky or fibrous
Metal particles	•Rich in metal elements such as Fe, Al, Ti, Zn, Ba, and Mg	•Small spherical aggregates with bright surface
Organic particles	•Predominantly C and O	•Mainly spherical or dome-shaped; easily decomposed under electron beams
Salt particles	•Predominantly Na and Cl	•Regular cubic or subcubic structures with smooth crystal surfaces
Soil dust	•Predominantly Si and Al, containing minor amounts of crustal elements such as Fe, Ca, and Mg	•Irregular flaky shape
Sulfur–calcium particles	•Predominantly S and Ca	•Tabular, prismatic or irregular shape
Sulfur-containing particles	•Rich in S	•Diverse morphologies, typically spherical or amorphous with relatively smooth surfaces

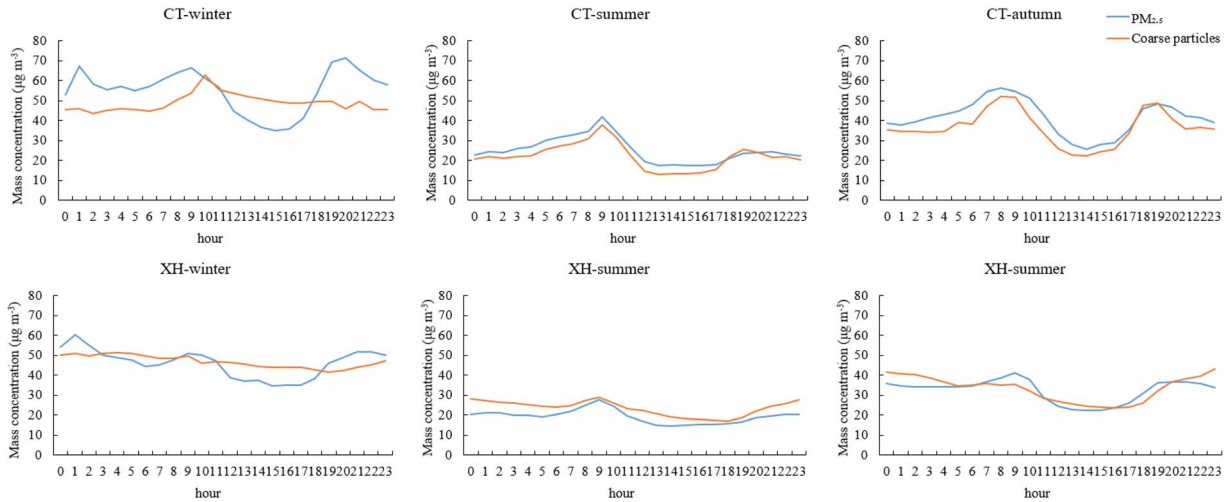

Fig. 2 Diurnal variation of particulate matter concentrations in different sampling periods of 2023 (winter, summer, and autumn from left to right).

coarse particles and $PM_{2.5}$ being 45.28 μg m^{-3} and 54.33 μg m^{-3}, respectively. In contrast, the lowest concentrations were observed in summer, where the average concentrations of coarse particles and $PM_{2.5}$ were 23.35 μg m^{-3} and 25.30 μg m^{-3}, respectively. The PM concentrations at the two sites during different sampling periods are presented in Table 1, which includes the duration of each individual sample and the corresponding concentrations of $PM_{2.5}$, coarse particles, and PM_{10}.

As shown in Fig. 2, the particulate matter concentrations exhibit a bimodal pattern throughout the day in most sampling periods, while the variation of coarse particle concentrations in winter is relatively stable. The peak concentration periods (*i.e.*, the two "peaks" of the bimodal pattern) are closely associated with human activities (*e.g.*, morning and evening rush hours of traffic, domestic fuel combustion, and industrial production shifts) and changes in the atmospheric boundary layer (*e.g.*, reduced mixing height in the early morning and late evening, which inhibits the diffusion of particulate matter).[27,28]

Size distributions

As illustrated in Fig. 3, coarse particles dominated the mass concentration contribution at both CT and XH across all sampling seasons, with the mass median diameter (MMD) generally ranging from 3 to 4 μm. Notable site-specific differences in size distribution characteristics were observed:

In CT, the MMD of the winter mass concentration size distribution shifted to approximately 2 μm a pattern closely associated with enhanced fine particle emissions from coal combustion for residential heating during the winter months. This fine-particle-dominated size distribution directly reflects the impact of local heating-related anthropogenic activities. In contrast, the MMD of particle mass concentration at the XH station remained stable at around 4 μm across all seasons. This consistency is attributed to persistent coarse particle inputs from surrounding mining activities, such as ore extraction, crushing, and on-site material handling, which continuously emit large quantities of coarse mineral particles.

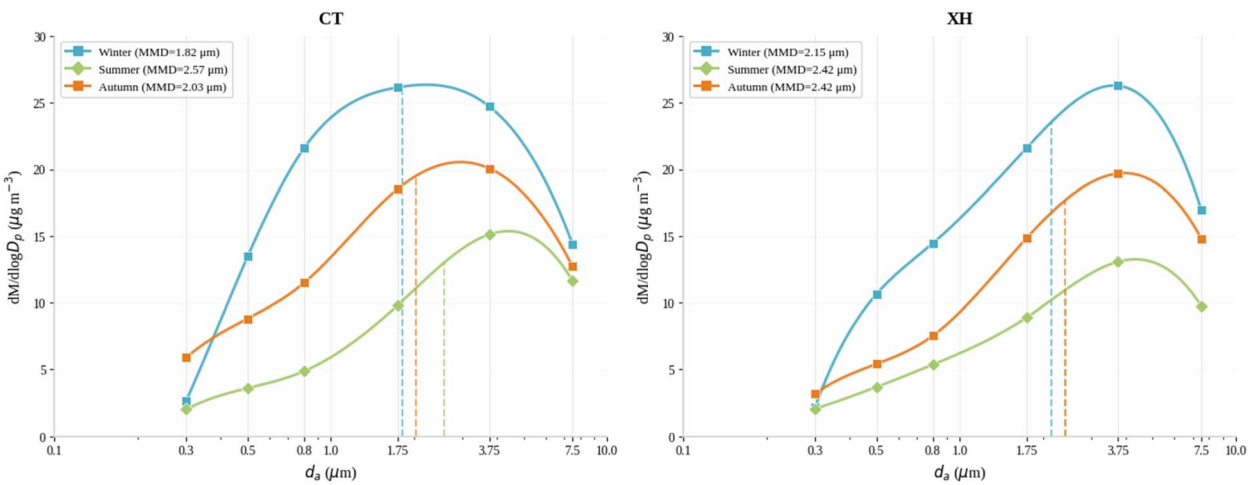

Fig. 3 Seasonal particle mass concentration size distributions at CT and XH.

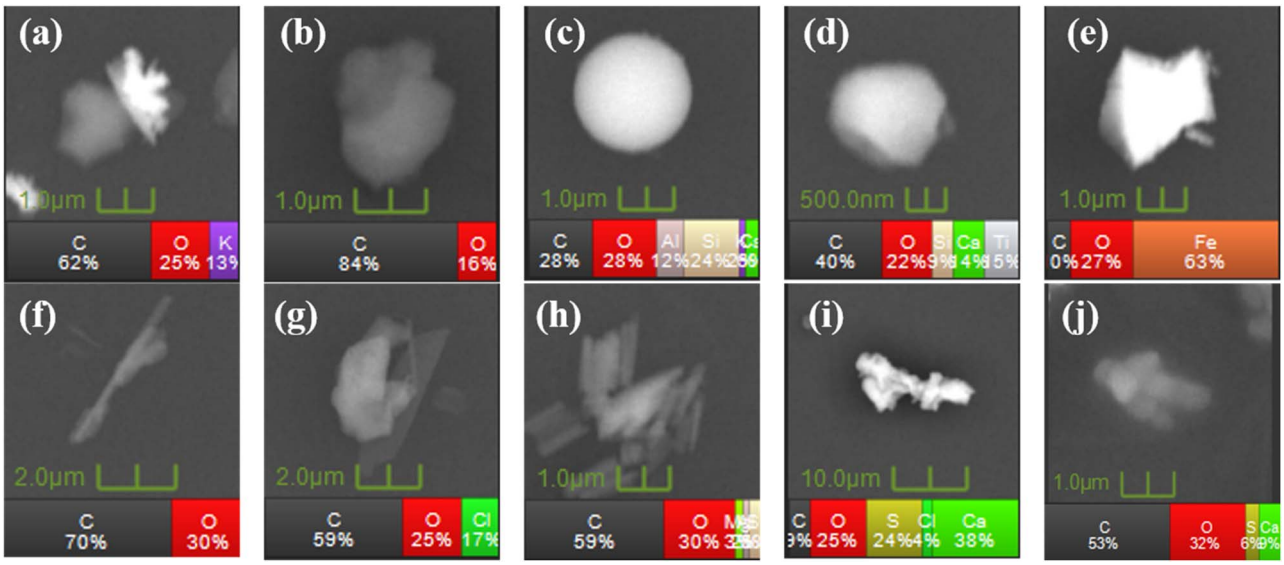

Fig. 4 Typical SEM images and EDS spectra of different source types by using an IntelliSEM-EPAS: (a) biomass particles; (b) carbonaceous particles; (c) coal-fired ash; (d) construction dust; (e) metal particles; (f) organic particles; (g) salt particles; (h) soil dust; (i) sulfur–calcium particles; (j) sulfur-containing particles.

Particle source types

As mentioned earlier, all ambient individual particles were ultimately classified into 10 major source types based on their morphological characteristics, particle sizes, chemical compositions, and potential sources. The characteristics of each type are discussed in the following sections.

Biomass particles. In this study, biomass particles accounted for 3.5% (Fig. 6) of the total particulate matter mass. Composed primarily of organic elements such as carbon (C) and oxygen (O), they may also contain trace minerals (*e.g.*, potassium (K) and calcium (Ca)). Under electron microscopy, biomass particles typically exhibit irregular morphologies with rough surfaces (Fig. 4(a)), and may possess fibrous or porous structures. These particles are mainly generated from sources including plant pollen, biomass combustion, and biomass energy production.

The results indicate (Fig. 5(a)) that the number concentration of biomass particles decreases with increasing particle size. Their mass size distribution is predominantly concentrated at around 0.5 μm, showing a unimodal pattern. At CT, a densely populated residential area, biomass particles are primarily emitted from the combustion of biomass fuels (*e.g.*, wood used for residential cooking). In contrast, relatively fewer biomass particles are generated in the vicinity of XH.

Carbonaceous particles. Carbonaceous particles accounted for 5.6% (Fig. 6) of the total particulate matter mass in this study. These particles have an amorphous structure composed of pure carbon (C), with small amounts of ash. Under electron microscopy, they typically appear as chain-like aggregates (Fig. 4(b)).

Carbonaceous particles are emitted from multiple sources, including combustion processes in steel mills and coking plants;[29] incomplete combustion during residential heating;[30,31] exhaust emissions from traffic sources.[32]

In terms of size distribution, the number concentration of carbonaceous particles is mainly concentrated in the fine particle range ($PM_{2.5}$) (Fig. 5(b)). In contrast, their mass concentration spans a relatively wide particle size range (1.0–8.0 μm) a characteristic attributed to the complex and diverse sources of carbonaceous particles.

Coal-fired ash. Coal-fired ash has a complex elemental composition: in addition to high contents of aluminum (Al) and silicon (Si), it may also contain various metal elements (*e.g.*, iron (Fe), calcium (Ca), magnesium (Mg), potassium (K), and sodium (Na)) and some non-metallic elements, exhibiting an overall characteristic of multi-element mixing.

Under a scanning electron microscope (SEM), coal-fired ash particles present a three-dimensional spherical morphology. These particles are mainly derived from various combustion processes, particularly fuel combustion in industrial activities. For instance, when fuels such as coal and heavy oil are burned, the high temperature generated melts the minerals contained in the fuels; subsequent rapid cooling of these molten droplets forms the spherical coal-fired fly ash particles observed.

In terms of size distribution, both the number concentration and mass concentration of coal-fired ash particles show a unimodal pattern. The peak of the number concentration is at around 0.5 μm, while the peak of the mass concentration is near 4 μm.

Construction dust. Construction dust is predominantly composed of calcium (Ca) an elemental composition closely linked to its main sources (*e.g.*, processing and use of cement, concrete, and mineral aggregates). Under scanning electron microscopy (SEM), these particles exhibit irregular morphologies, including blocky, flaky, or fibrous shapes.

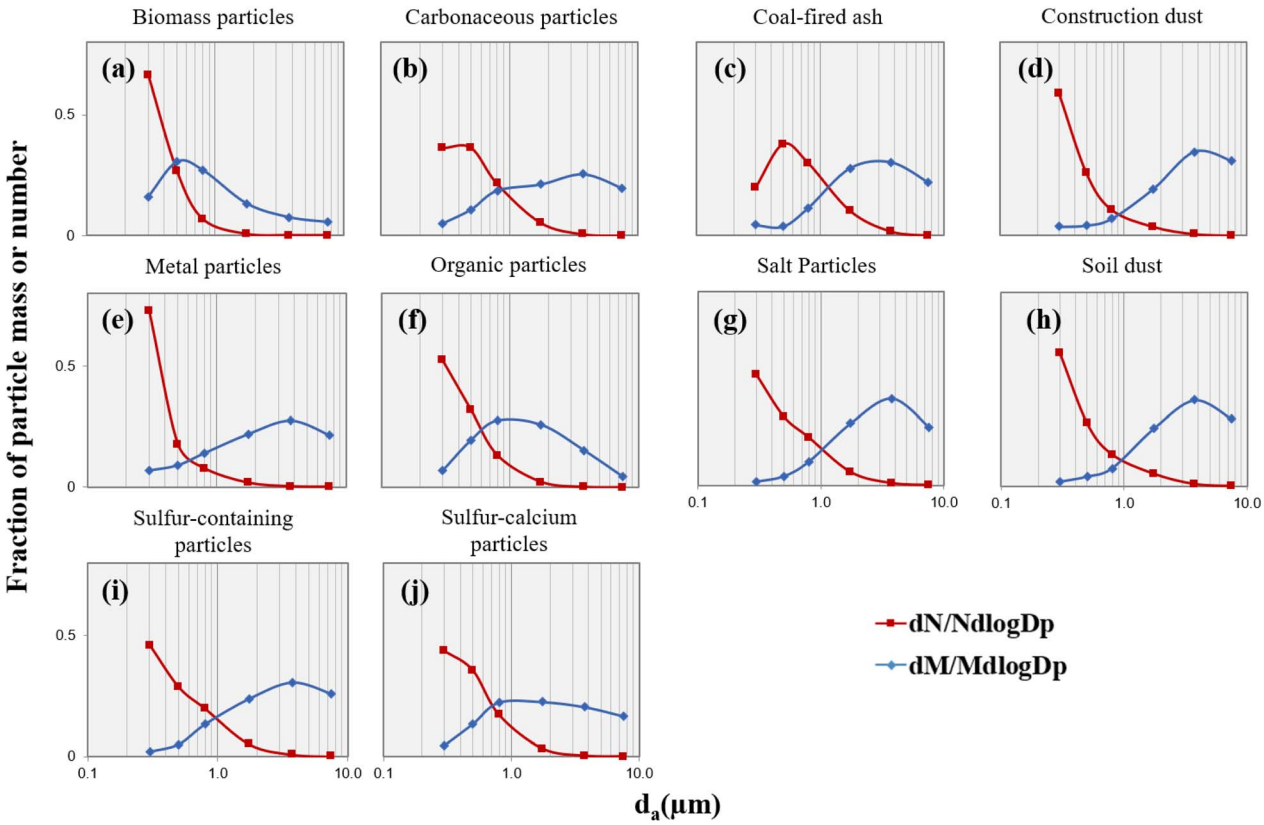

Fig. 5 Normalized mass and number size distributions of all 10 particle source types: (a) biomass particles; (b) carbonaceous particles; (c) coal-fired ash; (d) construction dust; (e) metal particles; (f) organic particles; (g) salt particles; (h) soil dust; (i) sulfur–calcium particles; (j) sulfur-containing particles.

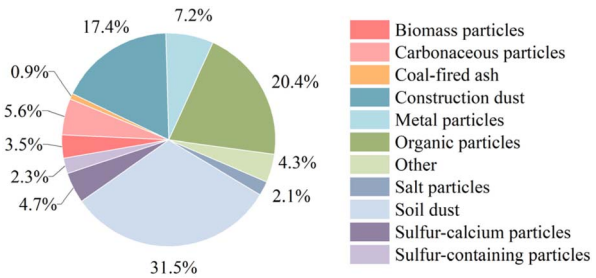

Fig. 6 Relative mass contributions of 10 particle types to all environmental particles.

In this study, construction dust accounted for 17.4% of the total particulate matter mass, making it the most dominant particle type-reflecting the significant impact of construction and mining-related activities on local particulate pollution. Its sources are mainly associated with construction activities, transportation, and stockpiling of building materials, and extraction, processing, and transportation of mining raw materials.[33]

Notably, the size distribution characteristics of construction dust are similar to those of soil dust. Both particle types show a broad size range, with mass concentrations primarily concentrated in the coarse particle segment.

Metal particles. Under a scanning electron microscope (SEM), metal particles typically appear as small spherical aggregates with bright surfaces. Energy-dispersive spectroscopy (EDS) analysis reveals that these particles are rich in metal elements such as iron (Fe), aluminum (Al), titanium (Ti), zinc (Zn), barium (Ba), and magnesium (Mg).

Metal particles originate from multiple processes, including iron and steel smelting; vehicle engine wear; iron ore mining and processing; mechanical equipment wear.

Regarding size distribution, the number concentration of metal particles shows a distinct peak at 0.3 μm, while their mass concentration forms a peak at around 4 μm.

Organic particles. Organic particles are primarily composed of carbon (C), oxygen (O), and small amounts of sulfur (S) and silicon (Si). Due to their high organic content, these particles are prone to decomposition under electron beams, which typically leads to an underestimation of their abundance in scanning electron microscopy (SEM) observations.[34]

In this study, organic particles accounted for 20.4% of the total particulate matter mass-representing one of the dominant particle types. Morphologically, they mainly exhibit spherical or dome-like shapes.

Organic particles are generated from two main pathways: direct release from anthropogenic activities such as vehicle exhaust and combustion processes; production as secondary

organic aerosols (SOA) *via* atmospheric oxidation reactions of volatile organic compounds (VOCs). Regarding size distribution, the number concentration of organic particles is concentrated in the particle size range below 1.0 μm, while their mass concentration reaches a peak between 0.8 and 2.0 μm.

Salt particles. Salt particles are primarily composed of sodium chloride (NaCl) as their core component, and may contain trace amounts of marine salts such as sulfate (SO_4^{2-}) and magnesium ions (Mg^{2+}). In many coastal cities and regions, salt particles account for a relatively high proportion of particulate matter (PM).[35] However, in northern China, deicing agents used in winter also serve as a significant source of such particles.[34]

Under electron microscopy, salt particles exhibit regular cubic or sub-cubic morphologies with smooth crystal surfaces. In this study, salt particles contributed 2.1% to the total particulate matter mass. Notably, the mass proportion of salt particles at both sampling stations (CT and XH) was higher in winter, indicating the significant contribution of deicing agents. Additionally, their mass size distribution was mainly concentrated at around 4 μm.

Soil dust. In this study, soil dust accounted for 31.5% of the total particulate matter mass. Its elemental composition is dominated by silicon (Si) and aluminum (Al), with trace amounts of iron (Fe) and magnesium (Mg) a signature consistent with the elemental profile of crustal materials, which are the primary components of soil.

Under scanning electron microscopy (SEM), soil dust particles primarily exhibit irregular flaky shapes, with rough surfaces often marked by scratches or adhering fine particles. This morphological feature is a result of physical weathering (*e.g.*, wind abrasion and water erosion) of crustal rocks and subsequent fragmentation, which disrupts the original crystal structure and forms irregularly shaped particles.

Soil dust in the study area is mainly derived from three pathways: wind erosion: resuspension of dust from bare land surrounding residential areas (*e.g.*, CT station) and mining operation zones (*e.g.*, XH station), particularly during dry and windy periods; road dust resuspension: turbulence generated by vehicle movement (*e.g.*, passenger cars in CT and mining trucks in XH) lifting accumulated soil particles from road surfaces; mining-related dust emissions: soil and rock fragmentation during mining activities (*e.g.*, ore excavation and waste rock stacking in XH) directly releasing coarse soil dust particles into the atmosphere.

Sulfur–calcium particles. Sulfur–calcium particles are compounds of sulfur (S) and calcium (Ca), with calcium sulfate ($CaSO_4$) being the most common form; they may also contain trace amounts of oxides.

Morphologically, these particles typically exhibit plate-like, prismatic, or irregular shapes, with distinct crystalline structures. Such particles are commonly found in industrial pollution zones and urban environments.

In the study area, sulfur–calcium particles accounted for 4.7% of the total particulate matter mass. Their mass concentration reached a peak within the particle size range of 0.8–1.0 μm, while their number concentration increased with decreasing particle size.

Sulfur-containing particles. Sulfur-containing particles are rich in sulfur (S) and exhibit diverse morphologies, typically appearing as spherical or amorphous particles with relatively smooth surfaces. Their sources are mainly associated with fossil fuel combustion and industrial exhaust emissions.

In terms of size distribution, the number concentration of sulfur-containing particles is primarily concentrated in the fine particle range ($PM_{2.5}$), while their mass concentration shows a significant peak at around 4 μm.

Notably, CT is adjacent to iron and steel plants and coking plants—industrial sources that burn fossil fuels (*e.g.*, coal) to generate large volumes of sulfur-rich exhaust, which further forms sulfur-containing particles. For XH, sulfur-containing gases are also released during coal mining and combustion

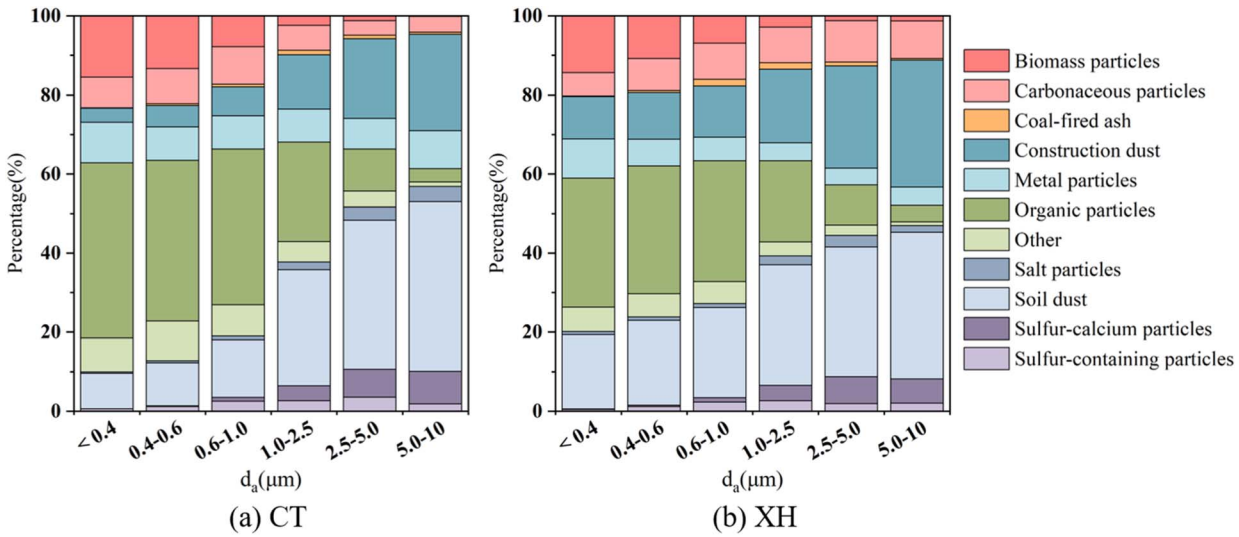

Fig. 7 Size-resolved mass proportions of different source types to all examined particles: (a) CT site; (b) XH site.

processes in the surrounding areas; these gases then undergo chemical reactions to form sulfur-containing particles. Additionally, exhaust emissions from mining transportation vehicles in the vicinity of XH may also contribute to such particles.

Source apportionment

Based on the particle classification results and their source analysis, the apportionment results of particles in any sample could be calculated. The size-resolved mass proportions of different source types to all examined particles are displayed in Fig. 7, and the mass source apportionment results of particles at CT and XH are shown in Fig. 8 and 9.

The contribution ratios of particles from different sources to particles in six size ranges were highly similar between the two sampling sites. Specifically, biomass particles, carbonaceous particles, metal particles, and organic particles-associated with combustion, industrial activities, vehicle exhaust, and secondary formation-accounted for a higher proportion in fine particulate matter than in coarse particulate matter. In contrast, construction dust, soil dust, and salt particles, which are closely linked to fugitive dust emissions, exhibited higher proportions in the coarse particle fractions. Both carbonaceous particles and sulfur-containing particles had a mass median diameter (MMD) ranging from 3 to 4 μm. Their contribution trends across different size ranges showed slight differences between the two sites, which could be attributed to the complex sources of these two particle types, along with the coexistence of their own aging processes and mixing with other particle species.

In summer, coal combustion decreased and precipitation events occurred more frequently, leading to the lowest particulate matter concentrations during the year. Although fugitive dust still accounted for a relatively high proportion of the total particles, its contribution to the overall concentration declined. In comparison, the fine particles closely related to combustion processes experienced a substantial reduction in both proportion and concentration in summer.

When comparing the two sampling sites, the trends of source contribution ratios and concentration variations across different particle sizes were generally similar (Fig. 7), but the specific contribution of each source showed significant differences. The $PM_{2.5}$ concentration at the CT site was notably higher than that at the XH site, mainly due to the higher concentration contributions from biomass particles, carbonaceous particles, metal particles, and organic particles. This phenomenon was closely associated with the dense residential areas adjacent to the site, as well as its proximity to steel mills and coking plants. In most cases, construction dust, soil dust, and salt particles contributed more to the $PM_{2.5}$ concentration at the XH site, which was linked to the intensive mining activities and fugitive dust emissions in the surrounding areas.

Overall, the particulate matter concentration levels and the source contributions at the two sites varied considerably across

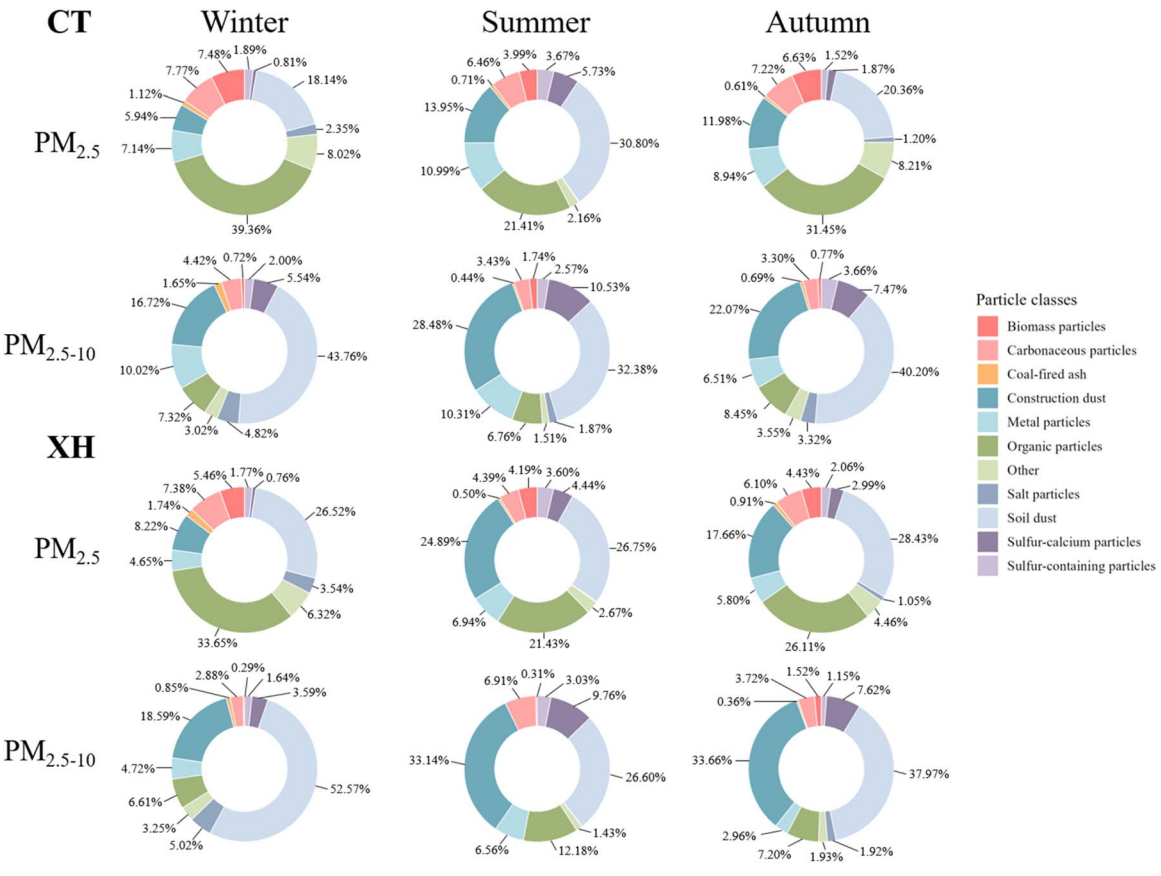

Fig. 8 Average mass contributions of different source types to $PM_{2.5}$ and coarse particles.

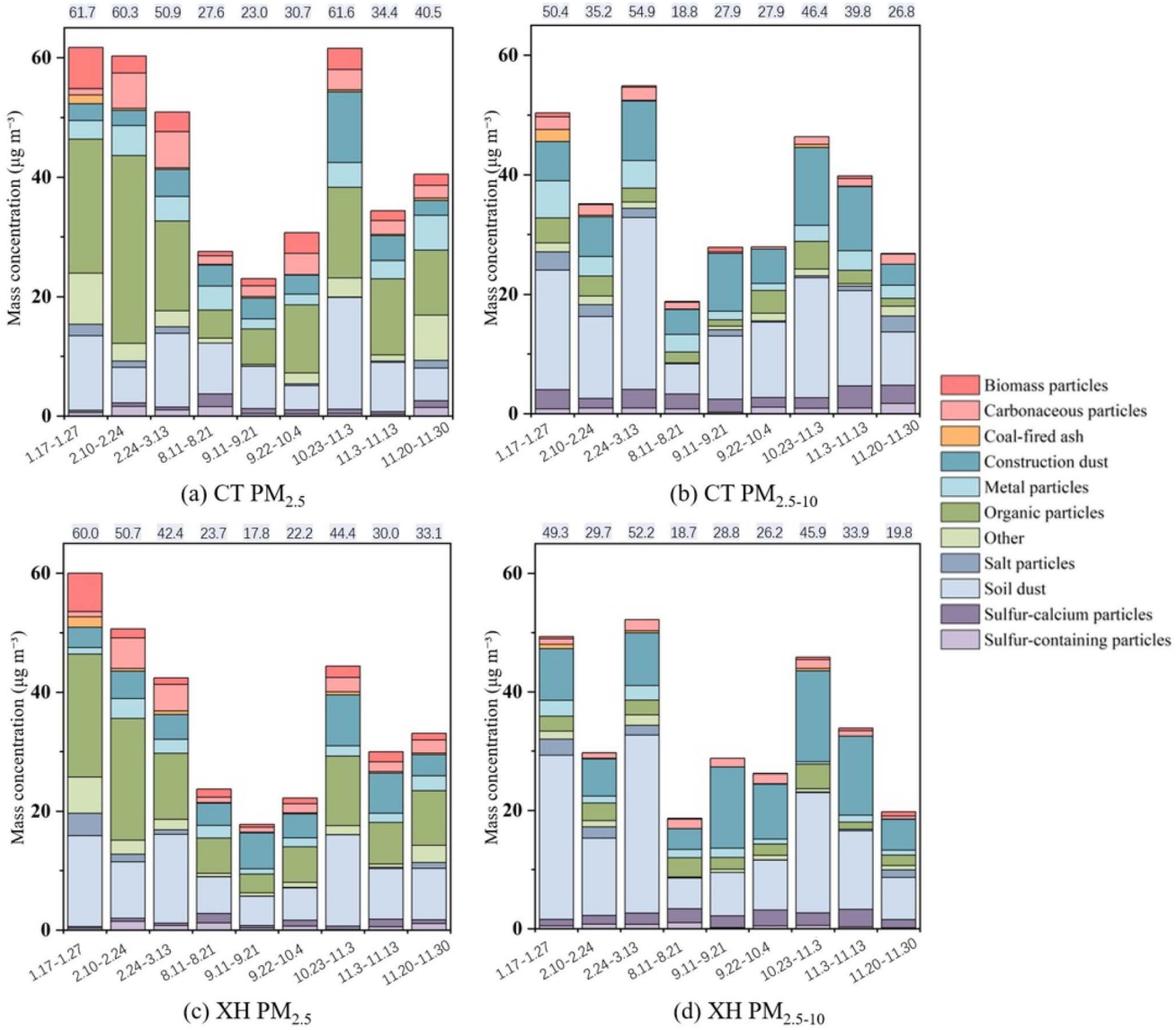

Fig. 9 Mass contributions of different source types to $PM_{2.5}$ and coarse particles for each sample: (a) $PM_{2.5}$ at CT; (b) coarse particles at CT; (c) $PM_{2.5}$ at XH; (d) coarse particles at XH.

different seasons, which were closely related to the distribution of pollution sources around the sampling sites and the prevailing meteorological conditions.

Conclusions

Based on CCSEM technology and big data-driven single-particle identification technology, this study conducted a systematic analysis of the characteristics and source apportionment of ambient particulate matter in Benxi across different seasons. The results demonstrated that the CCSEM single-particle analysis technology exhibits good applicability in typical heavy-industry cities like Benxi. Through the automatic identification and classification of a large number of ambient particles, morphology, size, and chemical composition of each individual particle were characterized, which verified the effectiveness and efficiency of this technology in the field of PM study.

Particulate pollution in Benxi shows significant seasonal and spatial variations. Particle concentrations displayed a seasonal pattern of being higher in winter and lower in summer, with the average $PM_{2.5}$ concentration reaching 45.28 μg m^{-3} in winter and dropping to a minimum of 23.35 μg m^{-3} in summer. The $PM_{2.5}$ concentration at the Caitun (CT) site was generally higher than that at the Xihu (XH) site, reflecting the combined impact of pollution from residential areas and industrial zones.

Soil dust and construction dust were identified as the primary local sources of particulate matter, accounting for 31.5% and 17.4% of the total mass respectively, which indicated the dominant role of fugitive dust sources in Benxi's PM pollution. This was followed by organic particulate matter (20.4%) and coal combustion ash (8.2%), reflecting the

significant impacts of industrial emissions, combustion processes, and secondary formation.

Particulate matter from different source types showed distinct size distribution characteristics. Biomass particles, sulfur-containing particles and organic particles, which are associated with combustion, industrial emissions, and secondary formation, were more concentrated in the fine particles. In contrast, fugitive dust sources such as soil dust and construction dust were mainly distributed in the coarse sizes.

There were obvious differences in source contributions between the two sampling sites. Affected by the surrounding steel mills, coking industries, and residential activities, the CT site showed prominent contributions from industrial and combustion sources (*e.g.*, metal particles and carbonaceous particles) in $PM_{2.5}$. In comparison, the XH site, influenced by mining and related transportation activities, had higher contributions from fugitive dust sources (*e.g.*, soil dust and construction dust) in the coarse size.

At present, the application of CCSEM technology for source identification of ambient particulate matter is still in its initial stage, and there remains considerable room for improvement in multiple aspects. For instance, in-depth research should be conducted on the single-particle characteristics of particulate matter emitted from different sources during various stages of generation, transportation, and transformation. A more comprehensive database of single-particle characteristics of sources across different regions should be established to provide a more scientific basis for source identification. Integration with other detection and analysis technologies is needed to improve the rationality and scientificity of source apportionment results. In addition, more advanced data processing methods should be applied to conduct in-depth mining of single-particle datasets.

Author contributions

Conceptualization: QL and PSZ. Data curation: QL, MHT, YTY and PSZ. Formal analysis: QL, MHT, and PSZ. Funding acquisition: QL and PSZ. Methodology: PZ and PSZ. Resources: PSZ. Writing – original draft: QL and MHT.

Conflicts of interest

The authors declare no conflicts of interest relevant to this study.

Data availability

Data for this article are available at the Science Data Bank at https://www.scidb.cn/detail?dataSetId=eeb2fc1e37824e71bf20483a1afb39fd.

Supplementary information (SI): CCSEM analysis details, particle classification methods, and introduction of passive sampler. See DOI: https://doi.org/10.1039/d6ea00012f.

Acknowledgements

This work was supported by the National Social Science Fund of China (22BTJ014).

References

1 P. K. Hopke, Review of receptor modeling methods for source apportionment, *J. Air Waste Manag. Assoc.*, 2016, **66**, 237–259.
2 Y. H. Zhu, L. Huang, J. Y. Li, Q. Ying, H. L. Zhang, X. G. Liu, H. Liao, N. Li, Z. X. Liu, Y. H. Mao, H. Fang and J. L. Hu, Sources of particulate matter in China: insights from source apportionment studies published in 1987–2017, *Environ. Int.*, 2018, **115**, 343–357.
3 M. Reizer, G. Calzolai, K. Maciejewska, J. A. G. Orza, L. Carraresi, F. Lucarelli and K. Juda-Rezler, Measurement report: receptor modeling for source identification of urban fine and coarse particulate matter using hourly elemental composition, *Atmos. Chem. Phys.*, 2021, **21**, 14471–14492.
4 D. Srivastava, J. S. Xu, T. V. Vu, D. Liu, L. J. Li, P. Q. Fu, S. Q. Hou, N. Moreno Palmerola, Z. B. Shi and R. M. Harrison, Insight into $PM_{2.5}$ sources by applying positive matrix factorization (PMF) at urban and rural sites of Beijing, *Atmos. Chem. Phys.*, 2021, **21**, 14703–14724.
5 I. Al-Naiema, A. D. Estillore, I. A. Mudunkotuwa, V. H. Grassian and E. A. Stone, Impacts of co-firing biomass on emissions of particulate matter to the atmosphere, *Fuel*, 2015, **162**, 111–120.
6 B. Moroni, D. Cappelletti, S. Crocchianti, S. Becagli, L. Caiazzo, R. Traversi, R. Udisti, M. Mazzola, K. Markowicz, C. Ritter and T. Zielinski, Morphochemical characteristics and mixing state of long range transported wildfire particles at ny-Ålesund (Svalbard Islands), *Atmos. Environ.*, 2017, **156**, 135–145.
7 W. J. Li, L. Y. Shao and P. R. Buseck, Haze types in Beijing and the influence of agricultural biomass burning, *Atmos. Chem. Phys.*, 2010, **10**, 8119–8130.
8 W. J. Li, A. Ito, G. C. Wang, M. K. Zhi, L. Xu, Q. Yuan, J. Zhang, L. Liu, F. Wu, A. Laskin, D. Z. Zhang, X. Y. Zhang, T. Zhu, J. M. Chen, N. Mihalopoulos, A. Bougiatioti, M. Kanakidou, G. H. Wang, H. L. Hu, Y. Zhao and Z. B. Shi, Aqueous-phase secondary organic aerosol formation on mineral dust, *Natl. Sci. Rev.*, 2025, **12**, nwaf221.
9 W. J. Li, L. Liu and L. Xu, Importance of Microanalysis in Air Quality Studies, in *Microanalysis of Atmospheric Particles: Techniques and Applications*, ed J. M. Conny, P. R. Buseck, American Geophysical Union, Washington, DC, 2024, pp. 55–74.
10 G. Casuccio, P. B. Janocko, R. J. Lee, J. Kelly, S. Dattner and J. S. Mgebroff, The use of computer controlled scanning electron microscopy in environmental studies, *J. Air Pollut. Control Assoc.*, 1983, **33**, 937–943.
11 A. P. Ault, T. M. Peters, E. J. Sawvel, G. S. Casuccio, R. D. Willis, G. A. Norris and V. H. Grassian, Single-

particle SEM-EDX analysis of iron-containing coarse particulate matter in an urban environment: sources and distribution of iron within Cleveland, Ohio, *Environ. Sci. Technol.*, 2012, **46**, 4331–4339.

12 P. C. Bernard, R. E. Van Grieken and D. Eisma, Classification of estuarine particles using automated electron microprobe analysis and multivariate techniques, *Environ. Sci. Technol.*, 1986, **20**, 467–473.

13 F. Karaca, I. Anil and A. Yildiz, Physicochemical and morphological characterization of atmospheric coarse particles by SEM/EDS in new urban central districts of a megacity, *Environ. Sci. Pollut. Res.*, 2019, **26**, 24020–24033.

14 R. D. Willis, F. T. Blanchard and T. L. Conner, *Guidelines for the Application of SEM/EDX Analytical Techniques to Particulate Matter Samples (Contract No.: 68-D-00-206)*. U.S. Environmental Protection Agency, North Carolina, 2002, https://nepis.epa.gov/Exe/ZyPURL.cgi?Dockey=P1005I40.TXT.

15 U. R. K. Lagudu, S. Raja, P. K. Hopke, D. C. Chalupa, M. J. Utell, G. Casuccio, T. L. Lersch and R. R. West, Heterogeneity of Coarse Particles in an Urban Area, *Environ. Sci. Technol.*, 2011, **45**, 3288–3296.

16 E. J. Sawvel, R. Willis, R. R. West, G. S. Casuccio, G. Norris, N. Kumar, D. Hammond and T. M. Peters, Passive sampling to capture the spatial variability of coarse particles by composition in Cleveland, OH, *Atmos. Environ.*, 2015, **105**, 61–69.

17 T. M. Peters, E. J. Sawvel, R. Willis, R. R. West and G. S. Casuccio, Performance of Passive Samplers Analyzed by Computer-Controlled Scanning Electron Microscopy to Measure $PM_{10\text{-}2.5}$, *Environ. Sci. Technol.*, 2016, **50**, 7581–7589.

18 T. F. Hu, F. Wu, Y. P. Song, S. X. Liu, J. Duan, Y. Q. Zhu, J. J. Cao and D. Z. Zhang, Morphology and mineralogical composition of sandblasting dust particles from the Taklimakan Desert, *Sci. Total Environ.*, 2022, **834**, 155315.

19 P. Zhao, P. S. Zhao, J. Tang, G. S. Casuccio, J. Gao, J. Li, Y. Y. He, M. Y. Li and Y. C. Feng, Source identification and apportionment of ambient particulate matter in Beijing using an advanced computer-controlled scanning electron microscopy (CCSEM) system, *Sci. Total Environ.*, 2022, **861**, 160608.

20 X. R. Kong, I. Staničić, V. Andersson, T. Mattisson and J. B. C. Pettersson, Phase recognition in SEM-EDX chemical maps using positive matrix factorization, *MethodsX*, 2023, **11**, 102384.

21 P. Zhao, P. S. Zhao, Z. W. Zhan, Q. L. Dai, G. S. Casuccio, J. Gao, J. Li, Y. Y. He, H. M. Qian, X. H. Bi, J. H. Wu, B. Jia, X. Liu and Y. C. Feng, Advancing Source Apportionment of Atmospheric Particles: Integrating Morphology, Size, and Chemistry Using Electron Microscopy Technology and Machine Learning, *Environ. Sci. Technol.*, 2025, **59**, 3645–3655.

22 P. Zhao, P. S. Zhao, W. Zhang, M. H. Tong, Y. T. Yang, G. S. Casuccio, L. Li, J. Gao, J. Li and Y. C. Feng, Source Identification of Atmospheric Particles via Low-Voltage Electron Microscopy Image Recognition: A Case Study of Submicrometer Particles, *Environ. Sci. Technol. Lett.*, 2026, **13**, 360–366.

23 J. Wagner and D. Leith, Passive Aerosol Sampler. Part I: Principle of Operation, *Aerosol Sci. Technol.*, 2001, **34**, 186–192.

24 M. D. Castillo, J. Wagner, G. S. Casuccio, R. R. West, F. R. Freedman, H. M. Eisl, Z. M. Wang, J. P. Yip and P. L. Kinney, Field testing a low-cost passive aerosol sampler for long-term measurement of ambient $PM_{2.5}$ concentrations and particle composition, *Atmos. Environ.*, 2019, **216**, 116905.

25 E. Coz and C. Leck, Morphology and state of mixture of atmospheric soot aggregates during the winter season over Southern Asia–a quantitative approach, *Tellus B*, 2011, **63**, 107–116.

26 P. Kumar, P. K. Hopke, S. Raja, G. Casuccio, T. L. Lersch and R. R. West, Characterization and heterogeneity of coarse particles across an urban area, *Atmos. Environ.*, 2012, **46**, 449–459.

27 W. Y. Xu, C. S. Zhao, L. Ran, Z. Z. Deng, P. F. Liu, N. Ma, W. L. Lin, X. B. Xu, P. Yan, X. He, J. Yu, W. D. Liang and L. L. Chen, Characteristics of pollutants and their correlation to meteorological conditions at a suburban site in the North China Plain, *Atmos. Chem. Phys.*, 2011, **11**, 4353–4369.

28 M. G. Li, L. L. Wang, J. D. Liu, W. K. Gao, T. Song, Y. Sun, L. Li, X. R. Li, Y. H. Wang, L. L. Liu, K. R. Daellenbach, P. J. Paasonen, V. M. Kerminen, M. Kulmala and Y. S. Wang, Exploring the regional pollution characteristics and meteorological formation mechanism of $PM_{2.5}$ in North China during 2013–2017, *Environ. Int.*, 2020, **134**, 105283.

29 K. Adachi and P. R. Buseck, Internally mixed soot, sulfates, and organic matter in aerosol particles from Mexico City, *Atmos. Chem. Phys.*, 2008, **8**, 6469–6481.

30 J. Li, M. Pósfai, P. V. Hobbs and P. R. Buseck, Individual aerosol particles from biomass burning in southern Africa: 2, compositions and aging of inorganic particles, *J. Geophys. Res. Atmos.*, 2003, **108**, 8484.

31 M. Pósfai, R. Simonics, J. Li, P. V. Hobbs and P. R. Buseck, Individual aerosol particles from biomass burning in southern Africa: 1. Compositions and size distributions of carbonaceous particles, *J. Geophys. Res. Atmos.*, 2003, **108**, 8484.

32 A. Smekens, R. H. M. Godoi, M. Vervoort, P. Van Espen, S. S. Potgieter-Vermaak and R. Van Grieken, Characterization of individual soot aggregates from different sources using image analysis, *J. Atmos. Chem.*, 2007, **56**, 211–223.

33 T. Siciliano, R. Giua, M. Siciliano, S. Di Giulio and A. Genga, The morphology and chemical composition of the urban PM_{10} near a steel plant in Apulia determined by scanning electron microscopy. Source apportionment, *Atmos. Res.*, 2021, **251**, 105416.

34 W. J. Li, L. Y. Shao, D. Z. Zhang, C. U. Ro, M. Hu, X. H. Bi, H. Geng, A. Matsuki, H. Y. Niu and J. M. Chen, A review of single aerosol particle studies in the atmosphere of East

Asia: morphology, mixing state, source, and heterogeneous reactions, *J. Clean. Prod.*, 2016, **112**, 1330–1349.

35 Y. K. Wong, K. M. Liu, C. Yeung, K. K. M. Leung and J. Z. Yu, Measurement report: characterization and source apportionment of coarse particulate matter in Hong Kong: insights into the constituents of unidentified mass and source origins in a coastal city in southern China, *Atmos. Chem. Phys.*, 2022, **22**, 5017–5031.